

A high-mobility hole bilayer in a germanium double quantum well

Alberto Tosato,¹ Beatrice M. Ferrari,¹ Amir Sammak,^{1,2} Alexander R. Hamilton,^{3,4} Menno Veldhorst,¹ Michele Virgilio,⁵ and Giordano Scappucci^{1,*}

¹*QuTech and Kavli Institute of Nanoscience, Delft University of Technology, PO Box 5046, 2600 GA Delft, The Netherlands*

²*QuTech and TNO, Stieltjesweg 1, 2628 CK Delft, The Netherlands*

³*School of Physics, University of New South Wales, Sydney, New South Wales 2052, Australia*

⁴*ARC Centre of Excellence for Future Low-Energy Electronics Technologies, University of New South Wales, Sydney, New South Wales 2052, Australia*

⁵*Dipartimento di Fisica "E. Fermi", Università di Pisa, Largo Pontecorvo 3, 56127 Pisa, Italy*
(Dated: January 19, 2022)

We design, fabricate, and study a hole bilayer in a strained germanium double quantum well. Magnetotransport characterisation of double quantum well field-effect transistors as a function of gate voltage reveals the population of two hole channels with a high combined mobility of $3.34 \times 10^5 \text{ cm}^2 \text{ V}^{-1} \text{ s}^{-1}$ and a low percolation density of $2.38 \times 10^{10} \text{ cm}^{-2}$. We resolve the individual population of the channels from the interference patterns of the Landau fan diagram. At a density of $2.0 \times 10^{11} \text{ cm}^{-2}$ the system is in resonance and we observe an anti-crossing of the first two bilayer subbands characterized by a symmetric-antisymmetric gap of $\sim 0.69 \text{ meV}$, in agreement with Schrödinger-Poisson simulations.

The development of high-quality undoped Ge/SiGe quantum wells [1, 2] has established planar Ge as a front-runner material platform en route to a large-scale spin-qubit quantum processor [3]. In only three years, key milestones have been demonstrated, such as stable and quiet quantum dots [2, 4], single hole qubits [5] with long relaxation times [6], singlet-triplet qubits [7], fast two-qubit logic [8], universal operation on a 2×2 qubit array [9], and simultaneous qubit driving at the fault-tolerant threshold [10]. Exploiting the third dimension by integrating two (or more) quantum wells in the same heterostructure could provide extra degrees of freedom for designing an entire new class of quantum device architectures with tailored electronic properties. For example, quantum devices patterned in multiple layers may provide increased qubit connectivity for high performance quantum circuits. In these devices, the wavefunction of quantum confined holes may be shifted or delocalized in between quantum wells, providing a larger parameter space for effective mass, g -factor, and spin-orbit coupling tuning [11]. These are relevant parameters for advanced spin-qubit control [3]. Furthermore, bilayers with high-mobility at low density may provide a suitable test bed for exploration of exotic phenomena such as exciton condensation [12, 13] and counterflow superconductivity in solid state devices at accessible temperatures [14, 15].

Here we demonstrate hole bilayers in planar Ge double quantum wells with high mobility at low density, a first prerequisite for exploring any of these exciting avenues. Through careful design of the heterostructure and because of the low disorder in both quantum wells, we are able to study in detail the quantum transport properties of the system in the tunnel coupled regime and observe the signature of a symmetric-antisymmetric gap when we tune the density in the quantum wells to be the same.

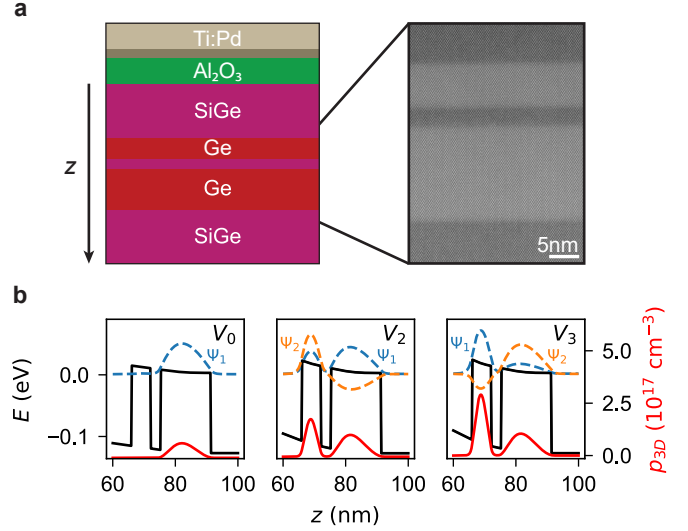


Figure 1. **a** Schematics of the Ge/SiGe heterostructure with the gate stack and cross section of the double quantum well by transmission electron microscopy. **b** From left to right at increasing negative gate voltage (V_0 , V_2 , and V_3), each panel shows the heavy-holes band edge (black solid line), the wavefunction of the subbands above the Fermi energy (colored dashed lines), and the total density $p_{3D} = p_1 |\Psi_1|^2 + p_2 |\Psi_2|^2$ (red solid line) vs. bilayer depth (z). Here Ψ_1 , Ψ_2 are the wavefunction amplitudes and p_1 , p_2 the densities of the first and second subband. The Fermi energy is set as the reference energy at 0 eV.

Figure 1a shows a schematics of the heterostructure, along with a cross section of the double quantum well by transmission electron microscopy. The Ge/SiGe bilayer was grown on a 100 mm Si(001) substrate in a high-throughput reduced-pressure chemical vapor deposition reactor [1]. The 16 nm bottom quantum well

and the 8nm top quantum well are separated by a thin 3nm $\text{Si}_{0.2}\text{Ge}_{0.8}$ barrier. The bilayer is grown on a strain-relaxed $\text{Si}_{0.2}\text{Ge}_{0.8}$ buffer layer obtained by reverse grading and is separated from the gate-stack by a 66nm $\text{Si}_{0.2}\text{Ge}_{0.8}$ barrier. The quantum wells are compressively strained, leading to states in the quantum wells with heavy hole (HH) symmetry being lower energy than light holes (LH) states.

The asymmetric design of the bilayer—the top quantum well being narrower than the bottom quantum well—allows both wells in the undoped heterostructure to be populated by applying a negative voltage to the top gate only [16]. We illustrate this capability in the three panels of Fig. 1b, which report the results of Schrödinger-Poisson (SP) simulations of our bilayer for increasing negative gate voltages. Each panel shows the HH-band-edge, the total hole density and the wavefunction amplitude for the first Ψ_1 and second Ψ_2 subband of the bilayer system, as a function of the spatial coordinate z . At small gate voltages ($V = V_0$, left panel), only the first subband is populated and its wave function Ψ_1 is localized in the bottom well. At larger gate voltages occupation of the second subband becomes favourable with its wavefunction Ψ_2 initially localized in the top well. Then, the energy of the second subband increases with gate voltage until it anticrosses the energy level of the first subband at the resonance point. The central panel ($V = V_2$) shows the system at resonance. In this regime, the wavefunction of the first and second energy states are delocalized across both wells giving rise to the symmetric Ψ_1 and antisymmetric Ψ_2 states characteristic of a tunnel-coupled double quantum well system. The energy separation between the symmetric and antisymmetric states reaches its minimum (Δ_{SAS}) at resonance. Upon further increasing the gate voltage ($V = V_3$ right panel), the wavefunction of the symmetric state shifts towards the top well and the total carrier density of the top quantum well increases while the one of the bottom quantum well remains unchanged.

We fabricated Hall-bar shaped heterostructure field effect transistors (H-FETs) featuring platinum-germanosilicide ohmic contacts [1] to the bilayer and performed measurements in a ^3He dilution refrigerator with base temperature of 50mK and equipped with a 12T magnet. Standard voltage-bias four-probe lock-in technique at a frequency of 17Hz was used for magnetotransport characterization as described in ref. [1]. We measure the longitudinal ρ_{xx} and transverse ρ_{xy} components of the resistivity tensor and via tensor inversion calculate the longitudinal σ_{xx} and transverse σ_{xy} conductivity.

The three panels of Fig. 2a show the zero-field longitudinal conductivity σ_{xx} , the bilayer density p and the carrier mobility μ as a function of gate voltage V_g . At turn-on, only the bottom quantum well is populated. Mobility, density, and conductivity increase monotonically as the

gate voltage is swept more negative up to a value $V_0 = -3.45\text{V}$. In particular the Hall density increases linearly, consistent with a parallel-plate capacitor model of an H-FET with a single quantum well [17]. We estimate a percolation density $p_p = 2.38 \times 10^{10}\text{cm}^{-2}$ by fitting the conductivity to percolation theory $\sigma_{xx} \sim (p - p_p)^{1.31}$ in the low density regime [18]. For $V_0 \leq V_g \leq V_1$ both the Hall density and conductivity deviate from the linear behaviour expected from SP simulations and flatten out. This observation signals that holes start populating the second subband; These holes are localized in the top quantum well, thereby screening the electric field at the bottom well. However, carriers in the top quantum well do not contribute to transport as their density is still below the percolation density. A further increase in negative gate voltage triggers transport in the top quantum well and for $V_1 \leq V_g \leq V_2$ we observe a transitory decrease in combined mobility due to inter-layer scattering [19]. For $V_g \geq V_2$ the combined mobility recovers its original monotonic increasing behaviour and saturates at $V_g = V_3$, reaching a maximum value $\mu = 3.34 \times 10^5\text{cm}^2\text{V}^{-1}\text{s}^{-1}$ at bilayer density $p = 2.21 \times 10^{11}\text{cm}^{-2}$.

To elucidate the quantum transport properties of the bilayer we show in the right panel of Fig 2a a colour map of σ_{xx} as a function of V_g and the inverse magnetic field B^{-1} . Dark regions correspond to filled Landau levels (LLs) with vanishing σ_{xx} and correspondingly quantized σ_{xy} . Bright lines correspond to sharp peaks in σ_{xx} at half-filled LLs. Line cuts of ρ_{xx} and σ_{xy} at $V_g = V_0, V_1, V_2$, and V_3 , are reported in Fig 2b as a function of magnetic field. For $V_g \leq V_0$, the conductivity color map reveals a LL fan diagram typical of a single subband 2DHG, with Zeeman splitting resolved at $B^{-1} < 2.5\text{T}^{-1}$. This is highlighted in line cuts at $V = V_0$: ρ_{xx} shows clean Shubnikov–de Haas (SdH) oscillations that vanish when σ_{xy} develops flat conductance plateaus at integer multiples of e^2/h .

For $V_0 \leq V_g \leq V_1$, the population of the second subband becomes favourable, charge starts accumulating in the top quantum well effectively screening the electric field in the bottom well. Although we observe the conductance peaks associated to the first subband saturating with gate voltage due to this screening effect, the fan diagram associated to the second subband appears only at $V_g = V_1$, in agreement with the observations in Fig. 2a, when the density in the second subband overcomes the percolation threshold and contributes to transport. Correspondingly, the line cuts for ρ_{xx} and σ_{xy} at $V_g = V_1$ show a complex pattern resulting from the parallel transport of two channels with different density and mobility.

The hole bilayer reaches the resonance point at $V_g = V_2$, corresponding to a bilayer density of $2.0 \times 10^{11}\text{cm}^{-2}$. At this point the wavefunction of the first and second subband are fully delocalized across both wells and we observe in the fan diagram the anticrossing of the σ_{xx} peaks

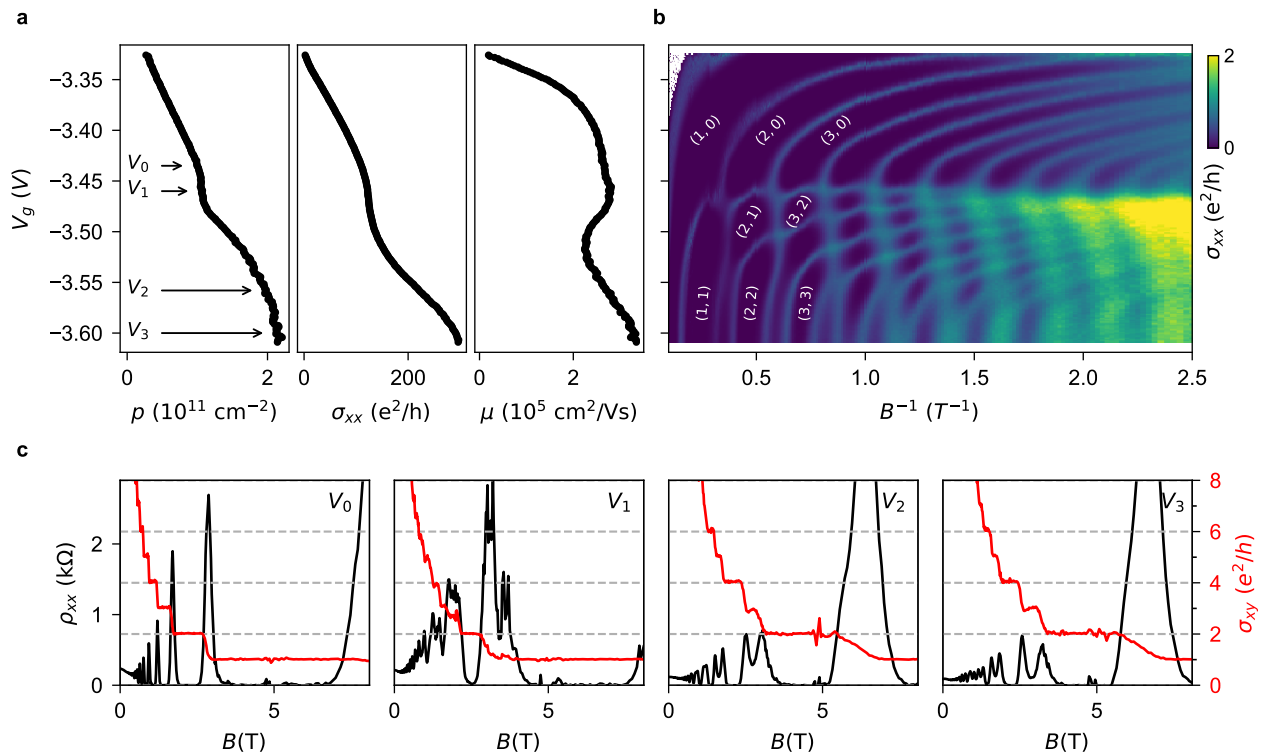


Figure 2. **a** From left to right: gate voltage (V_g) dependence of the hole bilayer Hall density p , conductivity σ_{xx} at zero magnetic field, and mobility μ . The bilayer behaviour at $V_g = V_0, V_1, V_2$, and V_3 is further described in the main text. **b** Colour map of the conductivity σ_{xx} as a function of V_g (same range as in **a**) and the inverse magnetic field B^{-1} . Dark regions correspond to filled Landau levels with vanishing σ_{xx} and correspondingly quantized σ_{xy} . In brackets the filling factor (ν_{sb1}, ν_{sb2}) for the first and second subbands where $\nu = 0$ indicates an empty subband. **c** From left to right: ρ_{xx} (black) and σ_{xy} (red) as a function of magnetic field B at $V_g = V_0, V_1, V_2$, and V_3 . These line cuts are obtained from the magnetotransport measurement in **b**. σ_{xy} shows plateaus at integer values of the total filling factor ($\nu_{sb1} + \nu_{sb2}$)

arising from the first subband with the corresponding peaks arising from the second subband. The anticrossing is better resolved at high magnetic field, where the LLs energy separation is large compared to the disorder-induced LLs broadening. The line cuts at resonance show a very distinct feature. A dip develops in ρ_{xx} in correspondence of the quantum Hall plateaus in σ_{xy} at odd filling factors 3, 5 and 7. This observation is a clear signature of the anticrossing of symmetric-antisymmetric subbands at the resonance point in a tunnel coupled bilayer system [20]. If the two quantum wells were not tunnel coupled, at resonance we would observe plateaus in σ_{xy} only at even filling factors and a doubling of the ρ_{xx} peaks height, arising from the measurement of two independent hole gases in parallel.

Finally, as the negative gate voltage is further increased beyond resonance, the energy separation between the symmetric and antisymmetric gap increases; the symmetric subband rises in energy (and thus hole density) and the antisymmetric state remains relatively unchanged due to electric field screening effect. The line cuts at $V_g = V_3$ show a larger ρ_{xx} peak separation in correspondence to larger odd Hall conductance plateaus. At

$V_g \approx -3.61$ V the bilayer system reaches its saturation as the triangular quantum well at the interface between the SiGe barrier and the dielectric starts populating, screening the electric field in both quantum wells from further increases in V_g .

A closer inspection of the fan diagram and line cuts reveals two interesting features of quantum transport in the bilayer. The first observation is about the development of the σ_{xx} peaks of the first subband in the color map. We note for $V_1 \leq V_g \leq V_2$ that an increase in negative V_g induces a shift of the peaks towards larger inverse magnetic field, implying that the charge in the first subband decreases as V_g is swept further negative. We ascribe this behaviour to the negative compressibility of the second subband [20]. When the charge density is still relatively low in the second subband, the first and second subbands are localized in the bottom and top quantum well, respectively. Making V_g more negative must increase the total density. The negative compressibility of the low density gas hole in the top quantum well causes the density in the bottom quantum well to decrease immediately after the top well is populated, explaining why the σ_{xx} peaks move to higher B^{-1} (lower B) in the region

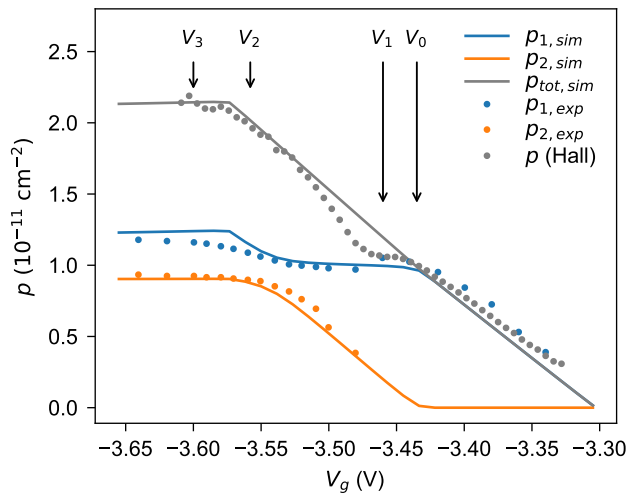


Figure 3. Comparison of the experimental and Schrödinger-Poisson simulated densities in the bilayer system as a function of gate voltage (V_g). The blue and orange solid lines are the simulated density for the first and second subband, respectively. The gray solid line is the simulated total density in the bilayer. The blue and orange dotted lines are the density of the first and second subband, as computed from the position of the Shubnikov-de Haas conductance peaks in Fig. 2b. The dotted gray line is the bilayer Hall density reported in Fig. 2a.

$V_1 \leq V_g \leq V_2$ [21, 22].

The second observation is about the emergence at resonance ($V_g = V_2$) of a quantum Hall state plateau at $\sigma_{xy} = 1e^2/h$. This dissipationless state could be ascribed either to the full occupation of the symmetric state while the antisymmetric one remains empty, or it could arise from a fractional quantum hall state. At such high magnetic fields (above 7 T), the intra-layer Coulomb energy $E_{intra} = e^2/\epsilon l_B$ (134 meV at 8 T) is much bigger than the tunneling energy Δ_{SAS} , as shown below, and the ratio of intra- to interlayer Coulomb energy $d/l_B = 0.76$ in our bilayer is less than two, suggesting that at resonance, the quantum Hall state at total $\nu = 1$ stems from spontaneous interlayer phase coherence [23]. Here, d is the distance between the centres of the two wells.

The accurate measurement of the LL fan diagram allows to compare in Fig. 3 the experimental density of the first and second subband to simulations [24]. We calculate the experimental subband density p_1 and p_2 using the quantum Hall relationship $p = \nu Be/h$ and tracking in Fig 2b the B position of the σ_{xx} peaks corresponding to the half filled LL with $\nu = 1.5$ [25]. We observe that the simulated subband population ($p_{1,sim}$, $p_{2,sim}$) matches well the experimental densities ($p_{1,exp}$, $p_{2,exp}$) in the ranges $V_g \leq V_0$ and $V_g \geq V_2$. SP calculations only include the Hartree contribution to many body effects, and so do not reproduce the negative compressibility effects observed in the range $V_1 \leq V_g \leq V_2$; we therefore expect a discrepancy between simulations and experimental data

in this region. Furthermore, in the range between V_0 and V_1 , we ascribe the deviation of the measured Hall density p from the simulated bilayer density $p_{tot,sim}$, to the population of the second subband when its density is still below the percolation threshold and effectively does not contribute to transport.

Around resonance ($V_g = V_2$) we observe the avoided-crossing of the simulated and experimental densities of the first and second subband. From the subband population difference at resonance $\Delta p_{SAS} = p_1 - p_2$ we calculate the experimental energy gap between the symmetric and antisymmetric subbands by dividing Δp_{SAS} by the spin-resolved 2D density of states $m^*/2\pi\hbar^2$. We obtain $\Delta_{SAS} \sim 0.69$ meV, which is in agreement with simulations.

In summary, we have designed, fabricated, and measured a hole bilayer in strained Ge double quantum wells. The bilayer has high-mobility, low percolation density, and a large symmetric-antisymmetric energy gap at resonance in agreement with simulations. Taken together, these results open up a plethora of exciting new possibilities for the Ge quantum information route, ranging from Ge quantum devices and circuits with increased connectivity to the exploration in this new platform of rich physics associated with quantum Hall effects in bilayers.

Data sets supporting the findings of this study are available at <https://doi.org/10.4121/17209091>

* g.scappucci@tudelft.nl

- [1] A. Sammak, D. Sabbagh, N. W. Hendrickx, M. Lodari, B. Paquelet Wuetz, A. Tosato, L. Yeoh, M. Bollani, M. Virgilio, M. A. Schubert, P. Zaumseil, G. Capellini, M. Veldhorst, and G. Scappucci, *Advanced Functional Materials* **29**, 1807613 (2019).
- [2] M. Lodari, N. W. Hendrickx, W. I. L. Lawrie, T.-K. Hsiao, L. M. K. Vandersypen, A. Sammak, M. Veldhorst, and G. Scappucci, *Materials for Quantum Technology* **1**, 011002 (2021).
- [3] G. Scappucci, C. Kloeffel, F. A. Zwanenburg, D. Loss, M. Myronov, J. J. Zhang, S. De Franceschi, G. Katsaros, and M. Veldhorst, *Nature Reviews Materials* **6**, 926–943 (2020).
- [4] N. W. Hendrickx, D. P. Franke, A. Sammak, M. Kouwenhoven, D. Sabbagh, L. Yeoh, R. Li, M. L. Tagliaferri, M. Virgilio, G. Capellini, G. Scappucci, and M. Veldhorst, *Nature Communications* **9**, 2835 (2018).
- [5] N. W. Hendrickx, W. I. Lawrie, L. Petit, A. Sammak, G. Scappucci, and M. Veldhorst, *Nature Communications* **11**, 3478 (2020).
- [6] W. I. Lawrie, H. G. Eenink, N. W. Hendrickx, J. M. Boter, L. Petit, S. V. Amitonov, M. Lodari, B. Paquelet Wuetz, C. Volk, S. G. Philips, G. Droulers, N. Kalhor, F. Van Riggelen, D. Brousse, A. Sammak, L. M. Vandersypen, G. Scappucci, and M. Veldhorst, *Applied Physics Letters* **116**, 80501 (2020).
- [7] D. Jirovec, A. Hofmann, A. Ballabio, P. M. Mutter, G. Tavani, M. Botifoll, A. Crippa, J. Kukucka, O. Sagi,

- F. Martins, J. Saez-Mollejo, I. Prieto, M. Borovkov, J. Arbiol, D. Chrastina, G. Isella, and G. Katsaros, *Nature Materials* **20**, 1106 (2021).
- [8] N. W. Hendrickx, D. P. Franke, A. Sammak, G. Scappucci, and M. Veldhorst, *Nature* **577**, 487 (2020).
- [9] N. W. Hendrickx, W. I. Lawrie, M. Russ, F. van Riggelen, S. L. de Snoo, R. N. Schouten, A. Sammak, G. Scappucci, and M. Veldhorst, *Nature* **591**, 580 (2021).
- [10] W. I. L. Lawrie, M. Russ, F. van Riggelen, N. W. Hendrickx, S. L. de Snoo, A. Sammak, G. Scappucci, and M. Veldhorst, Preprint at <https://arxiv.org/abs/2109.07837> (2021).
- [11] G. Burkard, G. Seelig, and D. Loss, *Physical Review B - Condensed Matter and Materials Physics* **62**, 2581 (2000).
- [12] J. P. Eisenstein and A. H. MacDonald, *Nature* **432**, 691 (2004).
- [13] J. J. Su and A. H. MacDonald, *Nature Physics* **4**, 799 (2008).
- [14] A. M. Rey, R. Sensarma, S. Fölling, M. Greiner, E. Demler, and M. D. Lukin, *EPL* **87** (2009).
- [15] S. Conti, S. Saberi-Pouya, A. Perali, M. Virgilio, F. M. Peeters, A. R. Hamilton, G. Scappucci, and D. Neilson, *npj Quantum Materials* **6**, 41 (2021).
- [16] D. Laroche, S. H. Huang, E. Nielsen, C. W. Liu, J. Y. Li, and T. M. Lu, *Applied Physics Letters* **106**, 143503 (2015).
- [17] J.-Y. Li, T.-M. Lu, Y.-H. Su, Y. Chuang, and C.-Y. Liu, *Physical Review Materials* **1**, 044601 (2017).
- [18] L. A. Tracy, E. H. Hwang, K. Eng, G. A. Ten Eyck, E. P. Nordberg, K. Childs, M. S. Carroll, M. P. Lilly, and S. Das Sarma, *Physical Review B* **79**, 235307 (2009).
- [19] H. L. Störmer, A. C. Gossard, and W. Wiegmann, *Solid State Communications* **41**, 707 (1982).
- [20] A. R. Hamilton, M. Y. Simmons, F. M. Bolton, N. K. Patel, I. S. Millard, J. T. Nicholls, D. A. Ritchie, and M. Pepper, *Physical Review B* **54**, R5259 (1996).
- [21] J. P. Eisenstein, L. N. Pfeiffer, and K. W. West, *Physical Review Letters* **68**, 674 (1992).
- [22] I. S. Millard, N. K. Patel, M. Y. Simmons, E. H. Linfield, D. A. Ritchie, G. A. Jones, and M. Pepper, *Applied Physics Letters* **68**, 3323 (1995).
- [23] K. Yang, K. Moon, L. Belkhir, H. Mori, S. Girvin, A. MacDonald, and L. Zheng, *Physical Review B - Condensed Matter and Materials Physics* **54**, 11644 (1996).
- [24] We performed iterative self-consistent SP simulations of this Ge/SiGe bilayer system. We set in the model the thicknesses of SiGe spacer above the bilayer and Al₂O₃, to match the saturation density and capacitance respectively, of the measured device.
- [25] Using the peaks of the half filled LL with $\nu = 2.5$ yields a very similar density.